Progress In Electromagnetics Research C, Vol. 27, 183–196, 2012

A TWO-PORT ANTENNA FOR WIRELESS-POWERED UWB-RFID TAGS

Y. Z. Shen* **and C. L. Law**

School of Electrical and Electronic Engineering, Nanyang Technological University, Singapore 639798, Singapore

Abstract—This paper presents a two-port antenna including a receiving port and a transmitting one in the same volume. These two antennas are physically integrated and electrically isolated. The receiving antenna is a linearly polarized narrowband slot for energy harvesting, whereas the transmitting one is a circularly-polarized ultrawideband (UWB) quasi-spiral for signal radiation. The measurement results show that, the slot resonates at 5.8 GHz, and the quasi-spiral has a 10-dB return loss bandwidth of 2.85–5.16 GHz and a 3-dB axial-ratio bandwidth of 3.05–4.43 GHz. The electrical isolation between these two antennas is more than 20 dB covering 1–8 GHz. This two-port antenna is a good candidate for wireless powered UWB-RFID tags.

1. INTRODUCTION

ULTRAWIDEBAND (UWB) technology paves the way to realize the next generation radio-frequency identification (RFID) systems with improved performances and additional capabilities [1]. In these UWB enabled RFID (UWB-RFID) systems, there are two categories: active [2–4] and passive chipless ones [5, 6]. Generally, an active UWB-RFID system can operate over long distance with enriched functionalities. However, it has higher tag cost due to the need for a battery and limited operation time without recharging the battery. On the other hand, a passive chipless tag has long lifetime but limited potential applications because there is no battery or chip.

To overcome the bottlenecks of these two kinds of UWB-RFID architectures, more recently, some research work is done on the wireless-powered (or remotely powered) UWB-RFID tags [7, 8]. As

Received 10 January 2012, Accepted 12 February 2012, Scheduled 20 February 2012
* Corresponding author: Yizhu Shen (sh0001hu@e.ntu.edu.sg).

illustrated in Fig. 1, many readers are involved for real-time localization and tracking. Different from the active [2–4] and passive chipless [5, 6] UWB-RFID systems, the wireless-powered system consists of two subsystems: a narrowband one and a UWB one. The narrowband 5.8 GHz subsystems are used to power on and off the UWB subsystem with modulated signals. Therefore, in this kind of system, the tag does not require a battery but still can work as an active tag, i.e., this tag is similar to an active one but battery-less. These wireless-powered UWB-RFID tags have many inherent advantages but also a defect: as illustrated in Fig. 2(a), the tag contains two separate antennas which occupy a large area.

In this paper, as shown in Fig. 2(b), a two-port antenna is proposed to replace the two separate antennas for wireless-powered UWB-RFID tags. It can receive a narrowband signal and transmit a UWB signal simultaneously. The narrowband antenna is used to receive signal for power up and data reception; while the UWB antenna provides short pulse transmission for UWB communication. It is also useful for cognitive radios [9].

Recently, UWB antenna with circularly polarized characteristics is becoming more and more popular, because it not only allows the flexible orientation of the transmitter and receiver, but also reduces the power loss due to the polarization mismatch. Circular polarization can be generated under this condition: two orthogonal and linearly polarized modes with equal amplitude but with 90° phase difference. There are mainly two kinds, i.e., the single-fed [10–13] and dual-fed [14, 15]. For example, in [10], by increasing the arm width of

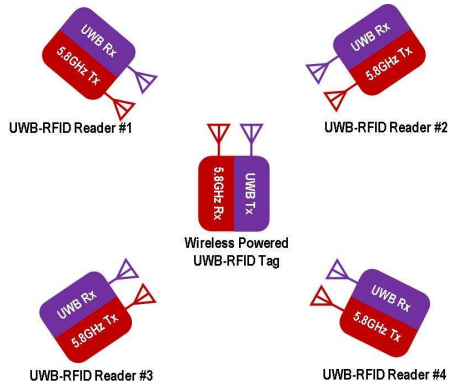

Figure 1. Conceptual illustration of a wireless powered UWB-RFID system.

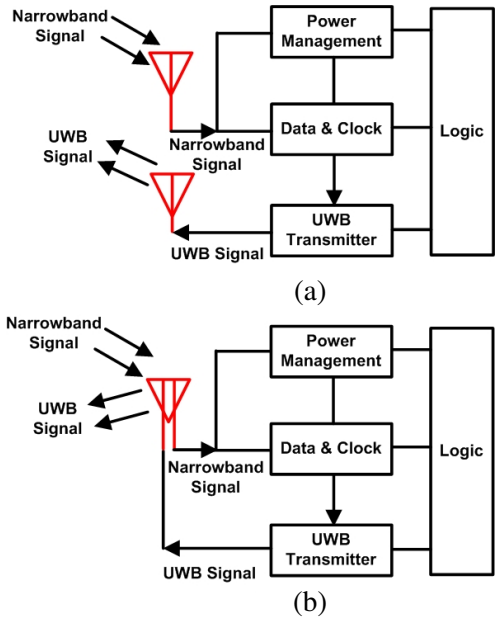

Figure 2. Block diagram of the wireless-powered UWB-RFID tags with different antenna topologies: (a) two separate antennas in [7, 8], and (b) the proposed two-port antenna.

original dipole antenna and using asymmetrical feeding structure, two perpendicular current distributions with 90° phase difference are obtained. Meanwhile, the circular polarization can also be excited by a so-called perturbation segment, like a widened L-type along the diagonal line of the square slot of antenna [11], a crisscross patch with proper dimensions embedded in the square slot [12], and a rectangular slot with 45° on the radiating patch [13]. However, the axial ratio bandwidths are not wide enough, only 27% [10], 17% [11], 12.4% [12], and 7.1% [13], respectively. On the contrary, dual-fed provides the possibility to obtain wider axial ratio bandwidth, but it requires an external polarizer like power splitter or hybrid coupler. In [14], a 90° broadband balun is employed to dually fed a microstrip antenna, and the axial ratio bandwidth is largely improved to 81.6%. Similarly, in [15], a three-stub hybrid coupler dual-fed antenna can realize 64.2% axial ratio bandwidth. Nevertheless, those dual-fed circularly polarized antennas are with complex structures and large size, due to the feeding network.

In this paper, a single-fed UWB antenna with improved axial ratio

bandwidth is designed. Moreover, a slot is introduced to perform as a linearly polarized narrowband antenna occupying the same volume as the UWB antenna. The details of the proposed dual function two-port antenna will be provided in the following sections.

2. ANTENNA DESIGN

As illustrated in Fig. 3, the proposed two-port antenna includes a narrowband slot for energy harvesting and a circularly-polarized quasi-spiral for UWB signal radiation. These two antennas are physically integrated on a Rogers (RO4003C, $\epsilon_r = 3.38$) substrate in the volume of 99 mm $\times$ 92 mm $\times$ 0.508 mm. The optimized antenna parameters in Fig. 3 are as follows: $w1 = 13$ mm, $w2 = 1$ mm, $w3 = 1$ mm, $w4 = 30.5$ mm, $w5 = 32$ mm, $L1 = 48$ mm, $L2 = 30.45$ mm, $L3 = 21.05$ mm, $Ls = 20$ mm, $s = 0.4$ mm, $g = 0.8$ mm, $g1 = 10$ mm, and $shift = 18$ mm. The detailed design procedures of these two antennas are described in the following sections.

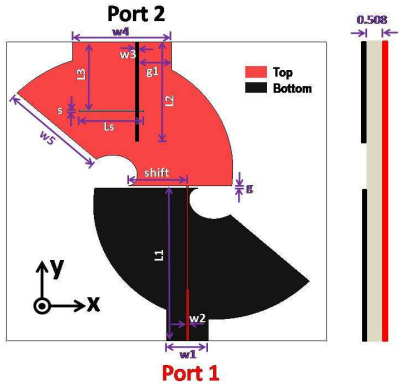

(a) top view and side view

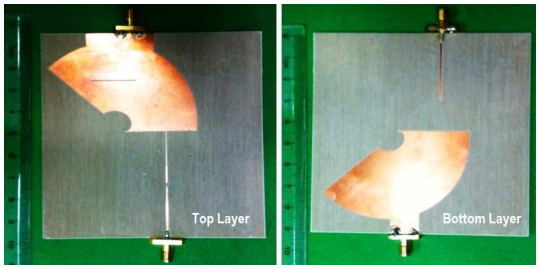

(b) prototype

Figure 3. Geometry and prototype of the proposed two-port antenna.

2.1. Circularly-Polarized UWB Quasi-Spiral Antenna

Spiral antennas [16–18] are widely investigated for UWB antenna designs because of the wide impedance bandwidth and inherent circularly-polarized radiation. Conventionally, a self-complimentary spiral antenna is complicated in the matching network due to its 188.5-Ω input impedance. Moreover, to feed two balanced arms of a spiral antenna, a wideband microstrip-to-coplanar stripline balun is needed.

In this section, a compact planar quasi-spiral antenna is developed and illustrated in Fig. 3. It is fed at port 1 when port 2 is terminated with a 50-Ω resistor. In a conventional Archimedean spiral, two arms are located on the same layer. While in our design, these two quasi-spiral arms are separately placed on the top and bottom layers of the substrate. It is found that the input impedance of this quasi-spiral antenna depends on the relative location of the two arms. By shifting the bottom arm along the x and $-y$ axis by 21.6 mm and 0.8 mm, respectively, the quasi-spiral antenna can be easily matched by a planar tapered microstrip line, which uses one spiral arm as the ground plane. This planar quasi-spiral is with simple feeding structure and is compatible with integrated circuits.

2.2. Linearly Polarized Narrowband Slot Antenna

Besides the above designed antenna, another important part of the two-port antenna is a narrowband antenna for harvesting energy. As shown in Fig. 3, a 20 mm × 0.4 mm slot is etched on the top arm of the quasi-spiral antenna. At port 2, a 50-Ω microstrip line with size of 30.45 mm × 1 mm is then employed to feed the narrow slot. The top arm is also used as the ground of the microstrip feedline. This narrow band slot antenna is designed to operate at 5.8 GHz with linear polarization.

2.3. Simulated Radiation Pattern of the Two-Port Antenna

Figure 3 shows the two-port antenna consists of the above designed quasi-spiral and narrowband slot antenna. When port 1 and port 2 of this two-port antenna are terminated with 50-Ω loads, respectively, the 3-D radiation patterns of the two individual antennas are presented in Fig. 4. It is interesting to note that, the main radiation lobes of the quasi-spiral and the narrowband slot are along the $-x$ axis and the $\pm z$ axis, respectively. This radiation characteristic is useful to reduce the mutual interference of the two physically integrated antennas.

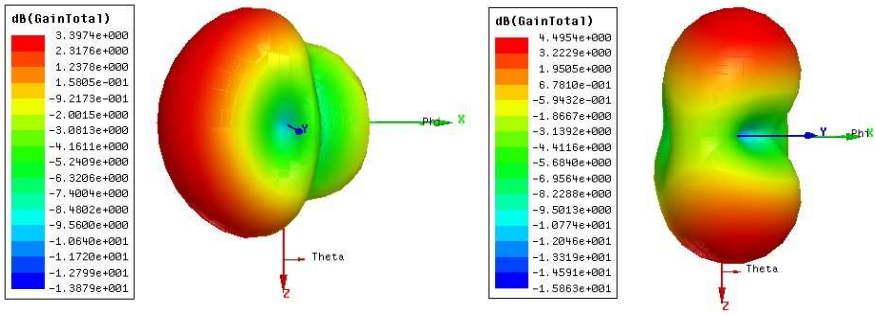

(a) (b)

Figure 4. Simulated 3-D radiation patterns of (a) UWB quasi-spiral antenna, and (b) 5.8 GHz narrowband slot antenna.

Table 1. The summary of varying $shift$ on the antenna performance.

$shift$	10 mm	14 mm	18 mm
10-dB Return Loss Bandwidth	2–4.1 GHz (68.9%)	2–4.2 GHz (70.9%)	1.95–5.15 GHz (90.14%)
3-dB Axial Ratio Bandwidth	3.4–4.2 GHz (21.1%)	3.32–4.38 GHz (27.5%)	3.35–4.66 GHz (32.7%)

3. PARAMETRIC STUDIES

In this section, some important parameters of this proposed two-port antenna are investigated, to see their influence on the antenna performance including the impedance matching as well as the axial ratio bandwidth. The parameter studies are simulated in Ansoft HFSS software, and all the other parameters that have not been mentioned are kept the same as stated in Section 2.

3.1. The Effect of the Feeding Position *Shift*

The proposed antenna employs a planar tapered microstrip line to feed the top arm, while using the bottom arm as the ground. It is found that the feeding position has significant influence on the $|S_{11}|$ and axial ratio bandwidth. As shown in Fig. 5, when the feeding position is shifted more and more to the right-hand side, both the impedance matching and axial ratio bandwidth become better. However, it should be mentioned that $shift = 18$ mm is the largest shifting distance, because the bottom arm is used as the ground of the microstrip feed. The summary of the effect of $s$hift is given in Table 1.

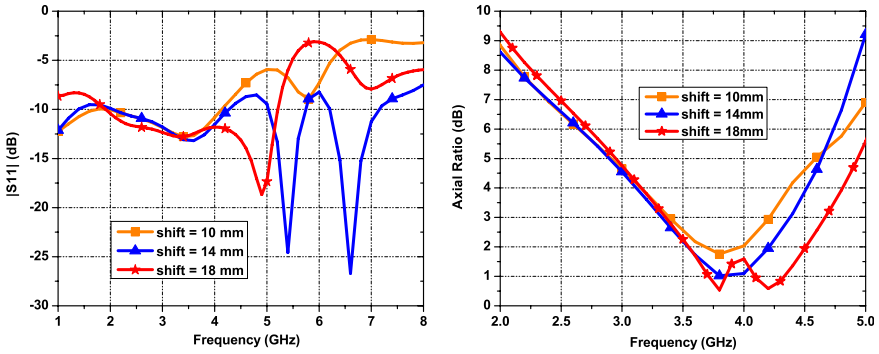

(a) (b)

Figure 5. Simulated results of the proposed antenna with varying the feeding position *shift*: (a) $|S_{11}|$, and (b) axial ratio.

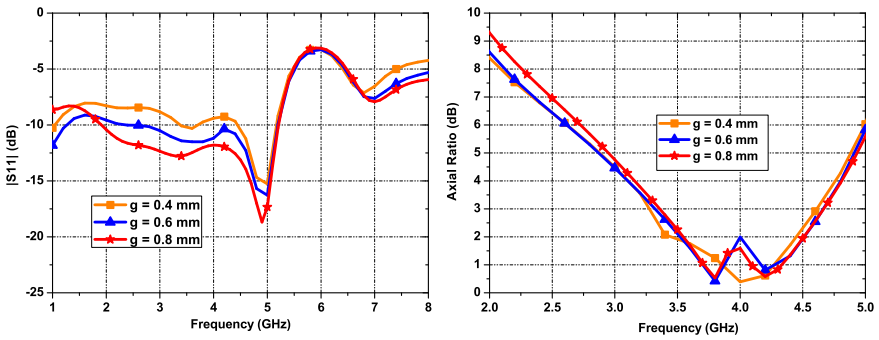

(a) (b)

Figure 6. Simulated results of the proposed antenna with varying the arm gap difference g: (a) $|S_{11}|$, and (b) axial ratio.

3.2. The Effect of Gap Difference between Two Arms g

Compared with conventional antenna, the bottom arm of the proposed antenna is shifted along the $-y$ axis with distance g. When g increases, it has large effect on the input impedance as shown in Fig. 6(a). Meanwhile, the axial ratio does not change much (see Fig. 6(b). except for a slight shift to a higher frequency. The details are shown in Table 2. Finally, $g = 0.8$ mm is chosen for the wide bandwidth.

3.3. The Effect of the Slot Width s

There is a 20 mm $\times$ 0.4 mm microstrip fed slot etched on the top radiation arm, used as a narrowband antenna resonant at 5.8 GHz for

Table 2. The summary of varying g on the antenna performance.

g	0.4 mm	0.6 mm	0.8 mm
10-dB Return Loss Bandwidth	4.41–5.2 GHz (16.4%)	2.8–5.2 GHz (60%)	1.95–5.15 GHz (90.14%)
3-dB Axial Ratio Bandwidth	3.28–4.61 GHz (33.7%)	3.31–4.67 GHz (34.1%)	3.35–4.66 GHz (32.7%)

Table 3. The summary of varying s on the antenna performance.

s	0.2 mm	0.4 mm	0.8 mm
10-dB Return Loss Bandwidth	5.4–5.7 GHz (5.4%)	5.55–5.9 GHz (6.1%)	5.7–6.1 GHz (6.8%)
Center Frequency	5.55 GHz	5.725 GHz	5.9 GHz

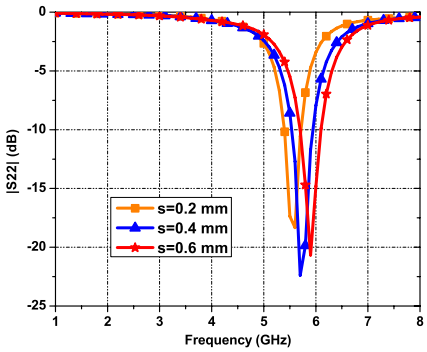

Figure 7. Simulated results of the proposed antenna with varying the slot size s.

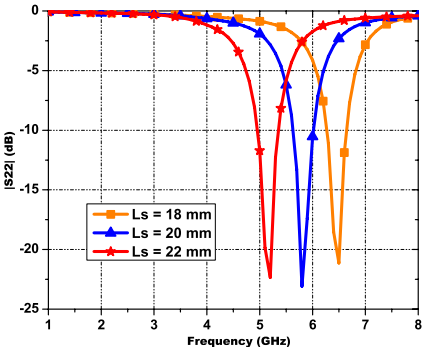

Figure 8. Simulated results of the proposed antenna with varying the slot size Ls.

harvesting energy in the UWB-RFID system. The width of the slot is also studied in Fig. 7 and Table 3. As s increases, the impedance bandwidth becomes wider, and the resonant frequency moves to high frequency. $s = 0.4$ mm is then employed for the desired frequency.

3.4. The Effect of the Slot Length *Ls*

The length of the slot is also important for the performance of the narrowband antenna. As shown in Fig. 8 and Table 4, the center frequency shifts to lower frequency when Ls increases, while the impedance bandwidth does not change much. 5.8 GHz resonant

Table 4. The summary of varying Ls on the antenna performance.

Ls	18 mm	20 mm	22 mm
10-dB Return Loss Bandwidth	6.3–6.6 GHz (4.65%)	5.65–6 GHz (6.1%)	4.95–5.35 GHz (7.8%)
Center Frequency	6.45 GHz	5.825 GHz	5.15 GHz

Table 5. The summary of varying $g1$ on the antenna performance.

$g1$	9 mm	10 mm	11 mm
10-dB Return Loss Bandwidth	NA (NA)	5.65–6 GHz (6.1%)	5.8–6.25 GHz (7.5%)
Center Frequency	NA	5.825 GHz	6.025 GHz

frequency can be obtained for energy harvesting with Ls chosen as 20 mm.

3.5. The Effect of the Slot Position $g1$

Figure 9 indicates that changing the feeding position of the microstrip line with respect to the slot results in feed impedance changes. The resonant frequency increases and the impedance bandwidth widens with increase of $g1$. The comparison of the effect is given in Table 5. The NA in the table means not applicable, since all results of $|S_{22}|$ are larger than -10 dB when $g1$ is equal to 9 mm.

4. MEASURED RESULTS AND DISCUSSIONS

After optimization discussed in Section 3, a prototype of the two-port antenna is then fabricated in-house, illustrated in Fig. 3(b), and measured.

4.1. S-parameters

S-parameters of the two-port antenna are measured using a vector network analyzer (Agilent N5244A). As presented in Fig. 10, the measured $|S_{11}|$ at port 1 shows that the quasi-spiral antenna has a 10-dB return loss bandwidth from 2.85 GHz to 5.16 GHz, about 57.7% of the center frequency of 4 GHz. The wideband operation ensures that it can transmit the lower band UWB signal in the wireless-powered system. Meanwhile, at port 2, the measured 10-dB return

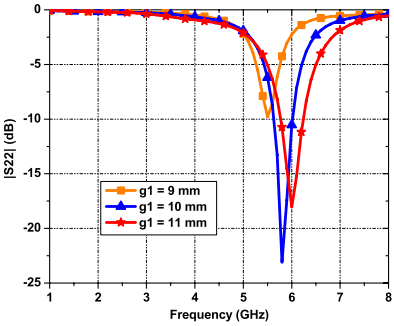

Figure 9. Simulated results of the proposed antenna with varying the slot size $g1$.

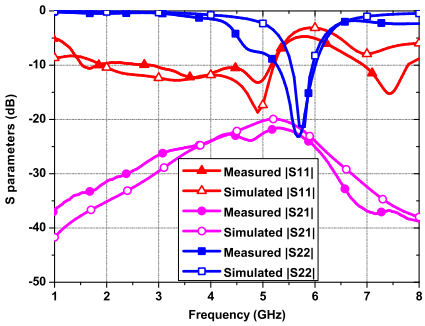

Figure 10. Simulated and measured S-parameters of the two-port antenna: the return loss at two ports $|S_{11}|$ and $|S_{22}|$, and the isolation between two ports $|S_{21}|$.

loss bandwidth also shows that the narrowband slot antenna resonates at 5.8 GHz. It can be used to receive a modulated 5.8 GHz signal for energy harvesting and clock generation.

The isolation coefficient between the two ports is shown in Fig. 10. Both the simulated and measured $|S_{21}|$ are less than -20 dB in the whole band of interest.

Generally, both simulated and measured two-port S-parameters are in good agreement. The difference may be due to the fabrication variation, and the simulation and measurement tolerance.

4.2. Axial Ratio Characteristics of Quasi-Spiral Antenna

Figure 11 shows that the measured 3-dB axial ratio bandwidth covers the range from 3.05 GHz to 4.43 GHz in boresight, with a factional bandwidth of 36.9%. This indicates that the proposed antenna can generate circularly-polarized radiation efficiently at the lower UWB band.

4.3. Radiation Pattern

Figure 12 illustrates the radiation patterns in xz-plane of the UWB quasi-spiral antenna at port 1 and the 5.8 GHz narrowband slot antenna at port 2.

Three frequencies in the first three figures, namely 3.5 GHz, 4 GHz, and 4.5 GHz, are chosen according to the impedance bandwidth of the UWB quasi-spiral antenna. At 4 GHz, the results show that the

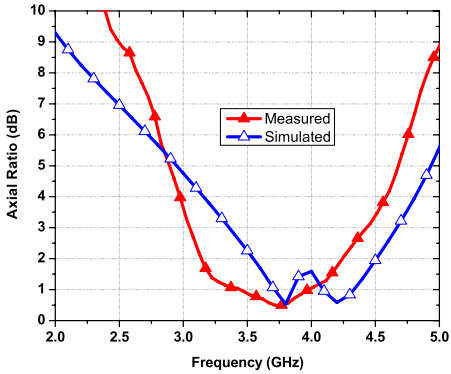

Figure 11. Simulated and measured axial ratio against frequency.

Table 6. Performance comparison of circularly polarized antennas.

Reference	Antenna Dimension	10-dB Return Loss Bandwidth	3-dB Axial Ratio Bandwidth
[10]	185×85 mm^2	1.25–1.75 GHz (33.3%)	1.67–2.2 GHz (27%)
[11]	100×100 mm^2	2.1–3.5 GHz (43%)	2.18–2.58 GHz (17%)
[12]	70×70 mm^2	1.604–2.45 GHz (39.6%)	1.84–2.08 GHz (12.4%)
This work	99×92 mm^2	2.85–5.16 GHz (57.7%)	3.05–4.43 GHz (36.9%)

quasi-spiral antenna radiates mainly towards the $-x$ axis, with 3 dB beamwidth of around 140°. The peak antenna gain is around 3.2 dBi. Fig. 12(d) presents the radiation pattern performance at port 2. Its maximum radiation is in the boresight of xz-plane, or both the positive and negative directions of the z-axis.

4.4. Comparison of the State-of-Art Antennas

Table 6 tabulates and summarizes the comparisons of the proposed two-port antenna in the circularly polarized performance with other reported ones. The proposed antenna achieves the highest impedance as well as the axial ratio bandwidth, and it is based on the single-fed method.

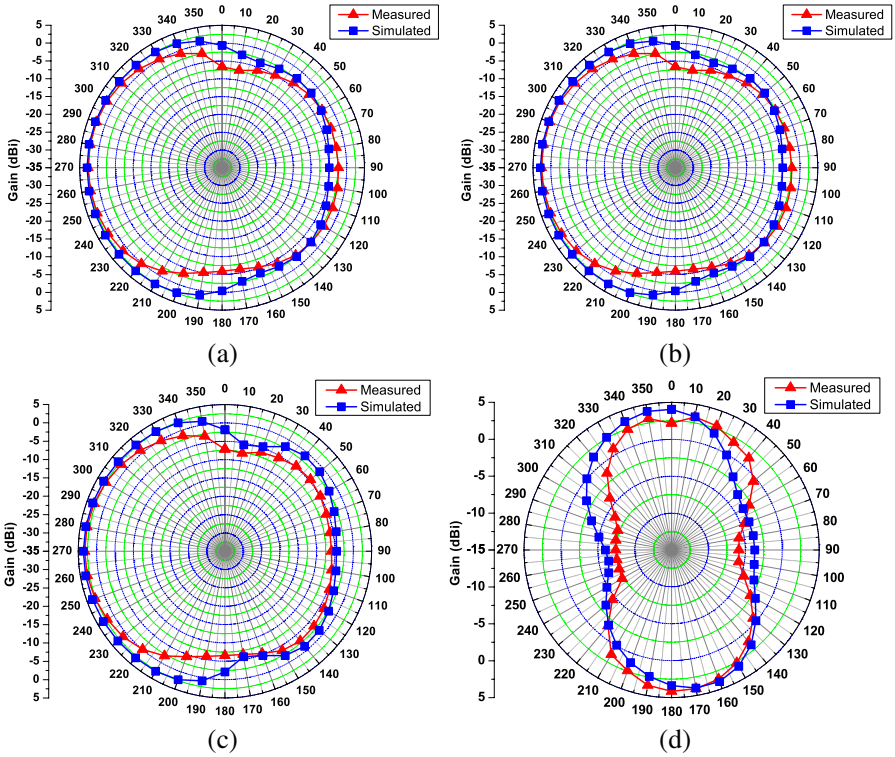

Figure 12. Simulated and measured xz-plane radiation pattern of the two-port antenna when its port 2 is terminated with a 50-Ω load: (a) 3.5 GHz, (b) 4 GHz, (c) 4.5 GHz. (d) shows the 5.8-GHz xz-plane radiation pattern of the two-port antenna when its port 1 is teminated with a 50-Ω load.

5. CONCLUSION

A two-port antenna is proposed and presented in this paper. It is composed of two different functional antennas, i.e., a narrowband slot antenna for energy harvesting and a circularly-polarized quasi-spiral antenna for UWB signal radiation, in the same physical volume and with high electrical isolation. Therefore, the volume is efficiently used. The numerical and experimental results are in good agreement, and demonstrate that the compact planar two-port antenna can simultaneously receive a modulated 5.8 GHz signal and transmit circularly-polarized UWB signal with isolation higher than 20 dB. This two-port antenna is a good candidate for wireless-powered UWB-RFID applications.

REFERENCES

1. Dardari, D., R. DErrico, C. Roblin, A. Sibille, and M. Z. Win, "Ultrawide bandwidth RFID: The next generation?" *Proc. IEEE*, Vol. 98, No. 9, 1570–1582, Sep. 2010.
2. Fontana, R. J., "Recent system applications of short-pulse ultrawideband (UWB) technology," *IEEE Trans. Microw. Theory Tech.*, Vol. 52, No. 9, 2087–2104, Sep. 2004.
3. http://www.ubisense.net/en/
4. Xia, J. J., C. L. Law, Y. Zhou, and K. S. Koh, "3–5 GHz UWB impulse radio transmitter and receiver MMIC optimized for long range precision wireless sensor networks," *IEEE Trans. Microw. Theory Tech.*, Vol. 58, No. 12, 4040–4051, Dec. 2010.
5. Hu, S., Y. Zhou, C. L. Law, and W. Dou, "Study of a uniplanar monopole antenna for passive chipless UWB-RFID localization system," *IEEE Trans. Antennas Propag.*, Vol. 58, No. 2, 271–278, Feb. 2010.
6. Ramos, A., A. Lazaro, D. Girbau, and R. Villarino, "Time-domain measurement of time-coded UWB chipless RFID tags," *Progress In Electromagnetics Research*, Vol. 96, 299–308, 2009.
7. Radiom, S., M. Maghaei-Nejad, K. Aghdam, G. A. E. Vandenbosch, L. R. Zheng, and G. G. G. Gielen, "Far-field on-chip antennas monolithically integrated in a wireless-powered 5.8-GHz downlink/UWB uplink RFID tag," *IEEE J. Solid-State Circuits*, Vol. 45, No. 9, 1746–1758, Sep. 2010.
8. Pelissier, M., J. Jantunen, B. Gomez, J. Arponen, G. Masson, S. Dia, J. Varteva, and M. Gary, "A 112 Mb/s full duplex remotely-powered impulse-UWB RFID transceiver for wireless NV-memory applications," *IEEE J. Solid-State Circuits*, Vol. 46, No. 4, 916–927, Apr. 2011.
9. Zhou, L. L., H. B. Zhu, and N. T. Zhang, "Iterative solution to the notched waveform design in cognitive ultra-wideband radio system," *Progress In Electromagnetics Research*, Vol. 75, 271–284, 2007.
10. Chi, L. P., S. S. Bor, S. M. Deng, C. L. Tsai, P. H. Juan, and K. W. Liu, "A wideband wide-strip dipole antenna for circularly polarized wave operations," *Progress In Electromagnetics Research*, Vol. 100, 69–82, 2010.
11. Chen, Y. B., X. F. Liu, Y. C. Jiao, and F. S. Zhang, "CPW-fed broadband circularly polarised square slot antenna," *Electronics Letters*, Vol. 42, No. 19, 1074–1076, Sep. 2006.

12. Chou, C. C., K. H. Lin, and H. L. Su, "Broadband circularly polarised cross-patch-loaded square slot antenna," *Electronics Letters*, Vol. 43, No. 9, 485–486, Apr. 2007.
13. Kasabegoudar, V. G. and K. J. Vinoy, "A broadband suspended microstrip antenna for circular polarization," *Progress In Electromagnetics Research*, Vol. 90, 353–368, 2009.
14. Guo, Y. X., K. W. Khoo, and L. C. Ong, "Ultra-wideband circularly polarized wide-slot antenna fed by three-stub hybrid coupler," *IEEE International Conference on Ultra-Wideband*, 487–490, 2007.
15. Qing, X. M., Z. N. Chen, and H. L. Chung, "Ultra-wideband circularly-polarized patch antenna," *Asia-Pacific Microwave Conference*, 1644–1646, 2006.
16. Liu, Q., C. L. Ruan, L. Peng, and W. X. Wu, "A novel compact archimedean spiral antenna with gap-loading," *Progress In Electromagnetics Research*, Vol. 3, 169–177, 2008.
17. Chen, T. K. and G. H. Huff, "Stripline-fed Archimedean spiral antenna," *IEEE Antennas Wireless Propag. Lett.*, Vol. 11, 346–349, 2011.
18. Eubanks, T. W. and K. Chang, "A compact parallel-plane perpendicular-current feed for a modified equiangular spiral antenna," *IEEE Antennas Wireless Propag. Lett.*, Vol. 58, 2193–2202, Jul. 2010.